IEEE Access
Multidisciplinary | Rapid Review | Open Access Journal

Received June 8, 2020, accepted June 18, 2020, date of publication July 1, 2020, date of current version July 16, 2020.

Digital Object Identifier 10.1109/ACCESS.2020.3006247

PAPR Reduction of OFDM Signal Through DFT Precoding and GMSK Pulse Shaping in Indoor VLC

RIZWANA AHMAD, (Member, IEEE), AND ANAND SRIVASTAVA, (Member, IEEE)
Department of Electronics and Communication, Indraprastha Institute of Information Technology Delhi (IIIT-D), New Delhi 110020, India
Corresponding author: Rizwana Ahmad (rizwanaa@iiitd.ac.in)

This work was supported by the Intel India Ph.D. Fellowship.

ABSTRACT Optical orthogonal-frequency-division-multiplexing (O-OFDM) has been widely explored for visible light communication (VLC) to achieve high data rates. However, O-OFDM suffers from high peak-to-average power ratio (PAPR), which causes clipping distortion, reduces illumination to communication conversion efficiency and affects the lifetime of the light-emitting diode (LED). This paper proposes a novel modulation technique, an amalgamation of discrete Fourier transform (DFT) precoding and Gaussian minimum shift keying (GMSK) pulse shaping to reduce the PAPR of OFDM based VLC system. Furthermore, the concept of group precoding is also introduced to deal with the increased complexity of the DFT precoding system. The results show that different variants of the proposed scheme provide improved PAPR, symbol-error-rate (SER), and power-saving performance as compared to the corresponding DFT precoded O-OFDM and O-OFDM counterpart. Moreover, the analytical study of PAPR, computational complexity and spectral efficiency for the proposed system have also been investigated and reported in this paper.

INDEX TERMS DFT-precoded OOFDM, double precoded O-OFDM (DP-OOFDM), Gaussian minimum shift keying (GMSK), optical-OFDM (O-OFDM), PAPR, real and imaginary separation, visible light communication (VLC).

I. INTRODUCTION

Cisco's survey reported that there would be a 7-fold increase in mobile data traffic from 2016 to 2021 [1]. This growing demand for wireless data transmission is making available radio frequency (RF) spectrum increasingly congested. In order to support future data traffic requirements, it is imperative to explore other parts of the electromagnetic spectrum for devising new communication technologies. One such option is Visible light communication (VLC), which utilizes visible light spectrum (380 to 780 nm) for short-range optical wireless communication. VLC is an attractive option for 5G wireless communication because of the following reasons [2], [3]: (a) it has huge unregulated spectrum (spectrum available is 10,000 times that of RF), (b) the light used for VLC is confined within the walls, therefore VLC provides inherent security and higher spatial reuse, (c) VLC is a green technology, since it is power efficient and utilizes the existing illumination infrastructure for communication, (d) it does not interfere with devices operating at 2.4 GHz, thus can be used as communication technology in aeroplanes and hospitals. Due to the above-stated reasons, VLC is expected to complement RF systems in future 5G technologies [4].

Orthogonal frequency division multiplexing (OFDM) is extensively used in wireless communication systems and has also been explored for VLC. VLC uses intensity modulation with direct detection (IM/DD) technique for data transmission in which the intensity of light from a light emitting diode (LED) transmitter is modulated according to the data to be transmitted. At the receiver, photodetector converts received optical signal into equivalent electrical signal for processing. For IM/DD communication, the transmitted signal must be real and positive. Therefore, in order to transmit complex bipolar OFDM signal over IM/DD optical system, it is essential to convert it into real and unipolar signal [5]. The complex OFDM signal is converted to real signal by using Hermitian symmetry. Furthermore, in order to obtain a unipolar OFDM signal, there are various techniques such as: a) DC biased optical OFDM (DCO-OFDM): DC bias is added to the bipolar OFDM signal,

The associate editor coordinating the review of this manuscript and approving it for publication was Fang Yang.

b) Asymmetrically clipped optical OFDM (ACO-OFDM): the bipolar signal is clipped at zero level and thus, only the positive part of the signal is transmitted, and c) Flip-OFDM: the positive and negative parts of the bipolar OFDM signal are extracted into two subframes, first subframe contains the positive part and second subframe contains the flipped negative part. These subframes are frame multiplexed to result into a frame having real unipolar values. ACO-OFDM is more power efficient compared to DCO-OFDM. However, DCO-OFDM outperforms ACO-OFDM in terms of spectral efficiency [6]. Flip-OFDM and ACO-OFDM have the same spectral efficiency [7]. The major drawback of OFDM based modulation is its high peak-to-average power ratio (PAPR), which causes clipping distortion, that results into degradation of system performance. In addition, a high PAPR reduces the illumination to communication conversion efficiency [8] and lifetime of the LED. In the next subsection we will summaries the literature related to PAPR reduction.

A. RELATED WORK

Several PAPR reduction techniques for optical OFDM (O-OFDM) have been investigated in the literature, which can be broadly classified into the following categories:

1) Signal Distortion Techniques: These techniques reduce the PAPR by distorting the O-OFDM signal before its transmission. Some common signal distortion techniques include (i) clipping and filtering [9], [10] (ii) companding [11] (iii) peak windowing [12] and (iv) peak reduction carrier. The clipping and filtering method works on the principle that high signal peaks occur rarely; therefore, these peaks can be clipped, which introduces signal distortion. Companding techniques involve the application of nonlinear transformation on the OFDM signal in order to reduce the PAPR values. However, this nonlinearity operation destroys the orthogonality of OFDM and results in degraded performance. These are simple to implement techniques, but they introduce clipping distortion, which results in SER degradation.
2) Multiple signalling and probabilistic techniques: These techniques generate multiple candidate signals that contain the same information, and the signal with the lowest PAPR is selected for transmission. Some common probabilistic techniques includes: (i) partial transmit sequences (PTS) [13], (ii) selected-mapping (SLM) [13], (iii) tone-reservation (TR) [14] and (iv) pilot-assisted (PA) [15]. Most of these methods typically require side information along with the data, which reduces the useful data rate and increases the computational complexity.
3) Precoding: One of the simplest methods for PAPR reduction is precoding [16]. In [17], authors proposed a block coding technique for PAPR reduction in O-OFDM; however, this technique requires additional bandwidth and introduces complexity overhead. In [18], authors proposed a discrete Hartley transform (DHT)-spread technique PAPR reduction in a DHT-based ACO-OFDM system. In [19], authors have considered precoding based on Vandermonde like matrix to reduce the high PAPR of DCO-OFDM and ACO-OFDM. In [20], authors have considered precoding based on discrete Fourier transform (DFT), DHT, and Zadoff-Chu transforms, and concluded that DFT precoder performs better than other precoders. It is found that DFT precoded OFDM provides lower PAPR and better bit error rate (BER) performance [21]. The benefit and feasibility of the DFT precoded OFDM modulation format for a Gbit/s VLC system are demonstrated in [22]. Meanwhile, in order to deal with the issue of substantial interference in DFT precoded OFDM, an optimized lighting layout was proposed in [23]. Further, it has also been shown in [24] that subcarrier waveform shaping in OFDM is a form of precoding scheme, where each OFDM block is linearly transformed by a shaping matrix before modulation and transmission. In literature, various pulse shaping filters like raised-cosine (RC), root-raised-cosine filter (RRC), Gaussian, and finite impulse response (FIR) Nyquist filters have been considered for low PAPR OFDM system [25]–[31]. In [32], authors have used partial response precoding based on Gaussian-minimum-shift-keying (GMSK) pulse for further PAPR reduction in DFT precoded OFDMA system.

The concept of Hermitian symmetry (HS) is used in O-OFDM to obtain a real signal. However, in [33], authors have demonstrated that due to the application of HS, only half of the time-domain DFT-precoded-OFDM symbols exhibit the single carrier form in VLC systems, therefore resulting in less compelling PAPR reduction as compared to radio counterparts. The inherent reason for this degradation is the loss of half of the degrees of freedom for subcarrier mapping due to the essential conjugate constraint for HS; this restricts the subcarrier mapping space to only half of the OFDM bandwidth after DFT operation, rather than the entire bandwidth as in RF systems. In [34], authors have implemented a HS free optical-single-carrier frequency-division multiple access (HSFO-SCFDMA) and illustrated that it performs better than other alternatives that utilises HS. Furthermore, in [35], authors have shown that implementation based on real and imaginary separation for DFT precoded layered ACO-OFDM provides better PAPR performance as compared to conventional the HS method.

B. MAIN CONTRIBUTIONS

In this paper, we propose a novel modulation technique based on GMSK pulse shaping and DFT-precoding to further reduce PAPR of the OFDM signal for the VLC system, without compromising the power efficiency of the system.

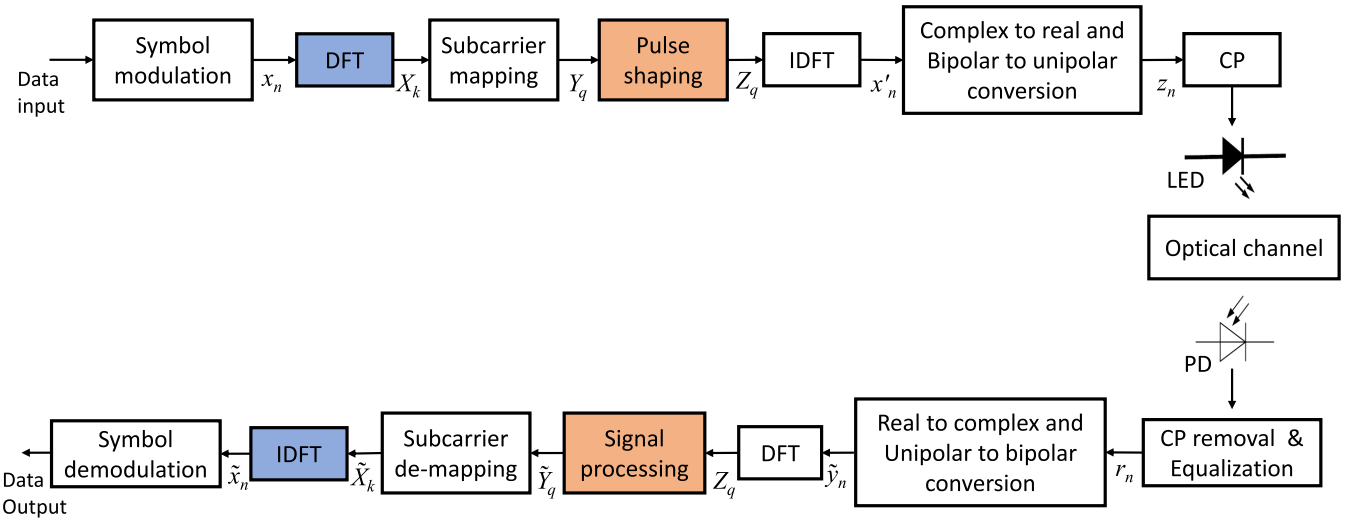

FIGURE 1. Block diagram of proposed scheme (DP-OOFDM).

Additionally, the concept of grouped precoding is also explored to reduce the computational complexity of the proposed scheme compared to conventional DFT precoding [36]. As two precoding operations are performed in this system, i.e., DFT precoding and GMSK pulse shaping; therefore, we have named the proposed scheme as double precoded O-OFDM: (DP-OOFDM). In order to make DP-OOFDM compatible with IM/DD the concept of real and imaginary separation and flip-OFDM have been implemented in this work instead of HS, as HS based DFT precoded O-OFDM does not provide the best PAPR reduction [33]–[35]. For pulse shaping, GMSK has been chosen because it provides constant envelope and high spectral efficiency [37]. Since the performance of flip-OFDM and ACO-OFDM is similar [7]. Therefore, the performance of the proposed DP-OOFDM has been evaluated against ACO-OFDM, based on PAPR, power saving, symbol error rate (SER), spectral efficiency, and computational complexity. To the best of our knowledge, the grouped DFT precoded OFDM based on real and imaginary part separation in conjunction with GMSK based pulse shaping has not been analyzed for VLC system. It may be noted that we have done limited work in [38], but that was restricted to the study of SER and PAPR performance. Furthermore, only the simplest (localized) subcarrier mapping was considered, which does not provide the best results in terms of PAPR. The main contributions of this paper are as follows:

1) The DP-OOFDM has been introduced which consist of grouped DFT precoded OFDM in conjunction with GMSK pulse shaping, this approach has resulted in lower PAPR and high spectral efficiency over earlier explored alternatives.
2) This work provides a comprehensive performance analysis of proposed DP-OOFDM in-terms of PAPR, power saving, SER, spectral efficiency and computational complexity against conventional DFT-precoded OOFDM and ACO-OFDM. For SER evaluation, a VLC channel with both line-of-sight (LOS) and non-line-of-sight (NLOS) components are considered.
3) The concept of grouped precoding is also explored for DP-OOFDM, in order to reduce the computational complexity of the proposed scheme compared to conventional DFT precoding. Further, different kinds of sub-carrier mapping has been analyzed to study the effect on PAPR and SER.
4) Analytical expression for PAPR of the proposed system is derived and compared with simulation results.

The rest of the paper is organized as follows: Section II describes the system model. Analysis of system complexity and spectral efficiency is summarized in section III, simulation results are presented in section IV and section V concludes the paper.

II. SYSTEM MODEL

The block diagram for the proposed scheme is shown in Fig.1. At the transmitter, symbol mapping block converts the input bits into one of several possible modulation formats like binary phase shift keying (BPSK), 4-level quadrature amplitude modulation (4-QAM) etc. The modulated symbols x_n, are grouped into blocks each containing N symbols. The N-point DFT is applied on this block of N symbols. In general, DFT is performed to transform the data from time domain to frequency domain. However, here N-point DFT is used as a precoder i.e., the block of N symbols are pre-coded using the DFT matrix to obtain X_k, as follows:

$$X_k = \frac{1}{\sqrt{N}} \sum_{i=1}^{N-1} x_n \exp^{\frac{-j2\pi ki}{N}}, \quad 0 \le k \le N \tag{1}$$

Further, subcarrier mapping block maps each of the N-point DFT outputs to one of the $M(> N)$ inputs of the inverse DFT (IDFT). There are two methods of subcarrier mapping; localized subcarrier mapping and distributed subcarrier mapping, details explained in section II-A. Factor of

$L(= M/N)$ defines the bandwidth expansion factor. For a system transmitting M symbols per block, L simultaneous transmissions are possible. The output of the subcarrier mapping is multiplied with frequency response of signal shaping waveform to obtain Y_q. Subsequently, M-point IDFT transforms the subcarrier amplitudes to a complex time domain signal x'_k. For IM/DD data transmission over optical wireless channel, the signal needs to be real and positive. The complex to real and bipolar to unipolar block makes the complex output of IDFT compatible for IM/DD transmission. Afterwards, cyclic prefix (CP) is added to z_n and resultant signal is transmitted by the LED. At the receiver, photodetector converts received optical power into electrical signal. After channel equalization and CP removal, real to complex and unipolar to bipolar block converts the real unipolar signal $\tilde{z}_n$ into complex bipolar signal $\tilde{y}_n$. Further, M-point DFT is applied followed by subcarrier de-mapping and frequency domain processing to reverse the signal shaping applied at the transmitter. The resulting signal is then subjected to N-point IDFT and symbol demodulation to obtain the data output corresponding to the transmitted input data. The following subsections discuss different subblocks of the system model.

A. SUBCARRIER MAPPING

Subcarrier mapping is achieved by implementing either the localized or distributed subcarrier mode. In localized mode, consecutive subcarriers are occupied by the DFT outputs of the input data whereas in the distributed mode, DFT outputs of the input data are allocated over the entire bandwidth with zeros occupying the unused subcarriers. Interleaved subcarrier mapping is a special case of distributed subcarrier mapping when $M = L \times$ âNĚN, therefore, equidistance subcarriers are occupied by DFT outputs of the input data [39]. The output of localized subcarrier mapping can be expressed as:

$$Y_q = \begin{cases} X_q : & q = 0, 1, \ldots, N-1 \\ 0 : & \text{otherwise} \end{cases} \tag{2}$$

Similarly, the output for interleaved subcarrier mapping can be expressed as:

$$Y_q = \begin{cases} X_{(q/L)} : & q = pL, \quad p = 0, 1, \ldots, N-1 \\ 0 : & \text{otherwise} \end{cases} \tag{3}$$

An example of localized and interleaved subcarrier mappings in the frequency domain for $M = 12$, $N = 4$, and $Q = 3$ is illustrated in Fig. 2.

Based on subcarrier mapping, the time domain output of IDFT differs i.e., samples equally spaced in frequency domain will result into periodic sequence in time domain and any shift in frequency domain will result into a phase rotation in time domain. Therefore, time domain output of IDFT for localized mode have exact copies of input time symbols at the M-multiple sample positions and the in-between values are complex weighted sum of all the time input symbols in the input block. Time domain output of IDFT for interleaved mode is simply a repetition of the original input symbols with a scaling factor and phase rotation. The time domain outputs of localized and interleaved mode are shown in Fig. 3. In this paper, we have analyzed the proposed system for both interleaved and localized subcarrier mapping.

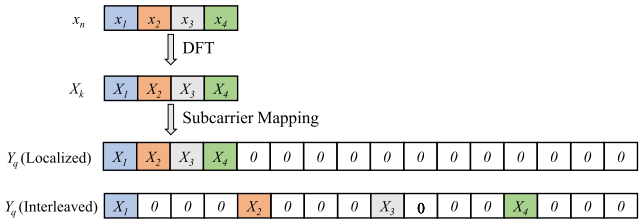

FIGURE 2. Subcarrier mapping in frequency domain.

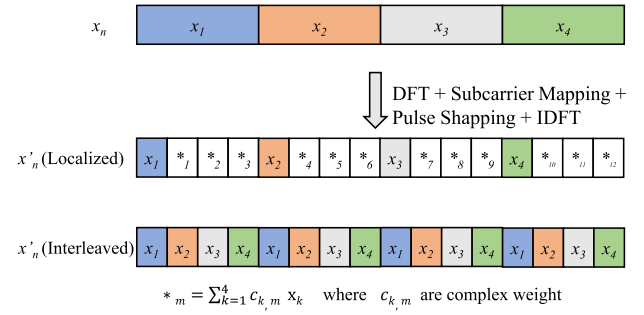

FIGURE 3. Time domain signal for different subcarrier mapping.

B. PULSE SHAPING

For a single carrier system, pulse shaping is required to band limit the transmitted signal. However, there is a trade-off between PAPR reduction and bandwidth efficiency in a single carrier system, i.e., pulse shaping limits the signal bandwidth at the cost of increased PAPR of the transmitted signals. In order to reduce the PAPR of the single carrier system, we need a pulse with a reduced tail size because the magnitudes of the filter's sidelobes directly affect the PAPR. Few studies have been carried out to design a pulse shaping filter that limits the signal bandwidth without degrading the PAPR performance [26], [27], [40]. In this paper, we have used GMSK filter for pulse shaping. GMSK pulse provides a constant envelope over the used bandwidth, and therefore improves the system performance. GMSK pulses are spectrally efficient and have reduced side lobe gain. Because of the aforementioned reasons, GMSK pulse has been chosen for pulse shaping in our proposed system. Further, for the sake of comparison with the conventional DFT precoded OFDM, we have considered rectangular pulse shaping filer as well which has been referred as DFT precoded OFDM in this paper. We have performed pulse shaping in frequency domain i.e.,

$$\mathbf{Z} = \mathbf{YS} \tag{4}$$

where $\mathbf{S}$ is the frequency response of the pulse shaping filter $g(t)$. The time domain pulse shaping filter $g(t)$ is defined as

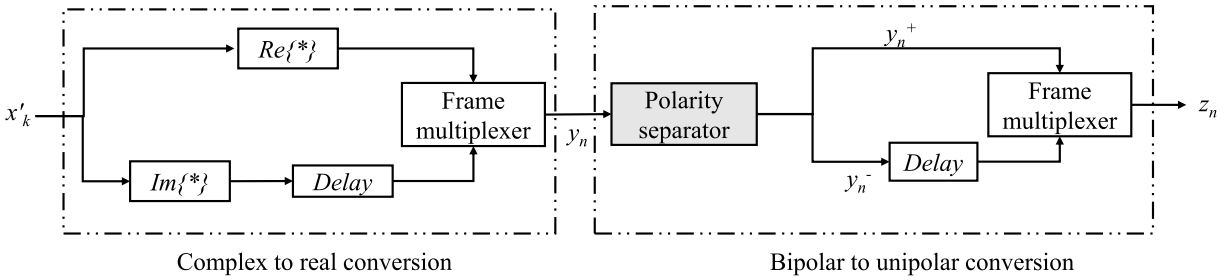

FIGURE 4. Complex to real and bipolar to unipolar conversion.

follows [32]:

$$g(t)_{GMSK} = \frac{1}{T}[Q(\gamma(\frac{t}{T} - \frac{1}{2})) - Q(\gamma(\frac{t}{T} + \frac{1}{2}))] \quad (5)$$

where $\gamma \approx \frac{2\pi BT}{\sqrt{ln(2)}}$, BT is the bandwidth time product, that controls the pulse shape, and $Q(x) \approx \frac{1}{2\pi}\int_x^\infty \exp(\frac{-u^2}{2})du$

$$g(t)_{Rect} = rect(\frac{t}{T}) = \begin{cases} 1 & \frac{-T}{2} < t < \frac{T}{2} \\ 0 & otherwise \end{cases} \quad (6)$$

C. COMPLEX TO REAL AND BIPOLAR TO UNIPOLAR CONVERSION

In order to transmit data using LED, the signal needs to be real and positive. To meet this requirement, generally HS is implemented, however, it is shown in [33]–[35] that HS degrades the PAPR performance for a DFT precoded system, therefore in this work, we have implemented real and imaginary separation, i.e., the real and imaginary part of the complex valued signal $\mathbf{x}'$ is separated and transmitted in different sub-frames. First sub-frame contains the real part of $\mathbf{x}$ i.e., $Re(\mathbf{x}')$ whereas, the second sub-frame contains the imaginary part i.e., $Imag(\mathbf{x}')$. After time multiplexing, the resultant vector $\mathbf{y}$ is represented as follows

$$y_n = \begin{cases} Re(x'_n): & 0 \le n \le M \\ Imag(x'_n): & M \le n \le 2M \end{cases} \quad (7)$$

The resultant bipolar signal y_n can be written as

$$y_n = y_n^+ - y_n^- \quad (8)$$

where, y_n^+ and y_n^- are the positive and negative parts of y_n respectively. Therefore uniploar z_n can be obtained as follows:

$$y_n^+ = \begin{cases} y_n: & y_n \ge 0 \\ 0: & \text{otherwise} \end{cases} \quad y_n^- = \begin{cases} |y_n|: & y_n \le 0 \\ 0: & \text{otherwise} \end{cases} \quad (9)$$

$$z_n = \begin{cases} y_n^+: & 0 \le n \le 2M \\ y_{n-2M}^-: & 2M \le n \le 4M \end{cases} \quad (10)$$

All the samples of the resultant signal z_n are unipolar which are transmitted through LED, as shown in Fig. 4.

D. GROUPED DFT PRECODING

The DFT precoding block adds extra computational complexity to the proposed system as compared to conventional optical OFDM system. One way to reduce this computational complexity is by using the concept of grouped precoding, where instead of performing N-point DFT, two $N/2$-point DFTs are applied. The N-block of data is divided into two $N/2$-blocks, each of which is processed by one of the two $N/2$-point DFTs. In this paper, we have analyzed the proposed system using both, simple (N-point) DFT precoding and grouped (two $N/2$-point) DFT precoding which are referred as DP-OOFDM and G-DP-OOFDM respectively.

E. OPTICAL CHANNEL

The indoor VLC optical channel is modeled by a linear time invariant (LTI) system with an impulse response of $h(t)$. The signal recieved at photo-detector is given by

$$y(t) = r \times h(t) * x(t) + n(t) \quad (11)$$

where $x(t)$ is the transmitted signal, r is the responsivity and $n(t)$ is the additive white Gaussian noise.

The impulse response $h(t)$ has two components namely h_{LOS} i.e., the impulse response of the line-of-sight (LOS) optical channel and h_{NLOS} i.e. the impulse response of the non-line-of-sight (NLOS) optical channel. Impulse response $h(t)$ can be expressed as

$$h(t) = h_{LOS}(t) + h_{NLOS}(t) \quad (12)$$

1) LOS LINK

h_{LOS} models direct LOS link between LED and PD and it can be written as [41]:

$$h_{LOS}(t) = \begin{cases} \frac{(m+1)A_d \cos^m(\varphi)\cos(\theta)\delta\left(t - \frac{d}{c}\right)}{2\pi d^2}: & \theta < \Phi \\ 0: & \theta > \Phi \end{cases} \quad (13)$$

where m is the mode number of the radiation lobe, A_d is the area of the PD, c is the speed of light, d is the distance between transmitter and receiver, Φ is the field of view of the receiver, θ is the angle of light incidence at the receiver and φ is angle of irradiance. The mode number m specifies the directionality of the source and can be calculated from the

source half-angle, α_H, which is defined as

$$\alpha_H = \arccos(0.5)^{\frac{1}{m}} \tag{14}$$

The angle of light incidence at the receiver is the angle of view (relative to normal direction) of the transmitter position when looking from the receiver, it can be expressed as:

$$\cos(\theta) = \widehat{n}_R \frac{(r_S - r_R)}{d} \tag{15}$$

The angle of irradiance is the angle of view (relative to normal direction) of the receiver position when looking from the transmitter, can be expressed as:

$$\cos(\varphi) = \widehat{n}_S \frac{(r_R - r_S)}{d} \tag{16}$$

where $\widehat{n}_S$ and $\widehat{n}_R$ are the orientations of the source and receiver respectively. The positions of source and receiver are r_S and r_R respectively.

2) NLOS LINK

h_{NLOS} considers the light rays reaching PD after being reflected from different walls of the room. $h_{NLOS}(t)$ is calculated by dividing each wall into K smaller reflecting surfaces, each with uniform area of ΔA and reflection coefficient of ρ. The over all impulse response of each ray reaching to PD is convolution of the impulse response of channel between LED and reflecting surface and the impulse response of channel between reflecting surface and PD. The resultant impulse response of the NLOS channel can be expressed as (17), shown at the bottom of this page, where φ_{Tk} is the angle between $\widehat{n}_S$ and d_{Tk}, and α_{Tk} is the angle between n_k and d_{Tk}, d_{Tk} is the distance between the LED source and the k^{th} reflecting surface, d_{Rk} is the distance between reflecting surface k of the wall and the PD, β_{Rk} is the angle between n_k and d_{Rk}, θ_{Rk} is the angle between $\widehat{n}_R$ and d_{Rk}, and n_k is the normal to the reflecting surface.

In the analysis, only first order reflection are taken into consideration as power received from higher order reflections is negligible [42]. In this paper, the focus is on the performance evaluation of the proposed scheme, therefore, for simplicity we have assumed φ and Φ equal to zero. The optical channel parameter are given in Table 1.

TABLE 1. Optical channel parameters.

Channel Parameter	Value
Mode number (m)	45
Area of receiver (A_d)	9.8 mm^2
Field of View (FOV)	60°
Responsivity ($\mathcal{R}$)	0.03 $\frac{A}{W}$

F. RECEIVER

At the receiver, photodetector receives optical signal and converts it into equivalent electrical signal. Afterwards, CP is removed and channel equalization is performed by a zero-forcing equalizer in order to compensate for distortion caused in transmitted signal due to the channel, resulting into signal r_n, which can be expressed as follows:

$$r_n = z_n + w_n \quad 0 \le n \le 4M \tag{18}$$

Further, a unipolar to bipolar and real to complex conversion block converts the real unipolar signal $\tilde{\mathbf{z}}_n$ into complex bipolar signal $\tilde{\mathbf{y}}_n$.

The bipolar signal $\tilde{z}_n$ is regenerated from r_n as

$$\tilde{z}_n = r_n - r_{n+2M} \quad 0 \le n \le 2M \tag{19}$$

Further, the real signal z_n can be converted into complex signal as follows:

$$\tilde{y}_n = \tilde{z}_n + j * \tilde{z}_{n+M} \quad 0 \le n \le M \tag{20}$$

Further, M-point DFT is applied to $\tilde{y}_n$, to obtain frequency domain transform $\tilde{Z}_k$.

$$\tilde{Z}_k = \frac{1}{\sqrt{M}} \sum_{i=1}^{M-1} \tilde{y}_n \exp^{\frac{-j2\pi ki}{M}}, \quad 0 \le k \le M \tag{21}$$

Afterwards, signal processing block and subcarrier demapping performs reverse operation of pulse shaping and subcarrier mapping respectively. The signal processing block performs following operation:

$$\tilde{\mathbf{Y}} = \tilde{\mathbf{Z}}/\mathbf{S} \tag{22}$$

The subcarrier demapping for localized mode can be expressed as:

$$\tilde{X}_n = \tilde{Y}_n \quad n = 0, 1, \ldots, N-1 \tag{23}$$

For interleaved mode subcarrier demapping can be obtained by:

$$\tilde{X}_n = \tilde{Y}_{nL} \quad n = 0, 1, \ldots, N-1 \tag{24}$$

Further, N-point IDFT is applied to convert the signal back into time domain, which is expressed as:

$$\tilde{x}_n = \frac{1}{\sqrt{N}} \sum_{i=1}^{N-1} \tilde{y}_n \exp^{\frac{j2\pi ki}{N}}, \quad 0 \le k \le N \tag{25}$$

Finally, symbol demodulation is applied in-order to obtain data output corresponding to data input.

$$h_{NLOS}(t) = \begin{cases} \dfrac{\sum_{k=1}^{K}(m+1)A_d\rho\cos^m(\varphi_{Tk})\Delta A\cos(\alpha_{Tk})\cos(\beta_{Rk})\cos(\theta_{Rk})\delta\left(t - \frac{d_{Tk}+d_{Rk})}{c}\right)}{2\pi d_{Tk}^2 d_{Rk}^2} : & (\theta_{Rk}) < \Phi \\ 0 : & (\theta_{Rk}) > \Phi \end{cases} \tag{17}$$

III. PERFORMANCE ANALYSIS AND COMPARISON

This section provides mathematical analysis and comparison of the DP-OOFDM with ACO-OFDM on the basis of PAPR, computational complexity and spectral efficiency.

A. PAPR ANALYSIS

The PAPR is defined as the ratio between the maximum peak power and the average power of the transmitted signal. PAPR of a transmitted signal z_n can be defined as

$$PAPR_z = \frac{\max\limits_{0\le n\le 4M-1} z_n^2}{E[z_n^2]} \tag{26}$$

where $E[\cdot]$ denotes the expectation operation. A high PAPR signal requires LEDs with large dynamic range in order to avoid clipping distortion. Additionally, high PAPR reduces illumination to communication conversion efficiency and lifetime of the LED. The probability of PAPR of block greater than the threshold value (ζ) is defined by complementary cumulative distribution function (CCDF). CCDF of PAPR is commonly used to measure the performance of PAPR reduction techniques. The PAPR of ACO-OFDM can be expressed as [43]:

$$\begin{aligned}\Gamma_{ACO-OFDM} &= \text{Prob}(PAPR > \zeta)\\ &= \begin{cases} 1-[2\phi(\sqrt{c(0,u)\zeta}-1)]^{\frac{M}{2}}, & 0\le\zeta\le\theta_{0,U}\\ 0, & \zeta\ge\theta_{0,U}\end{cases}\end{aligned} \tag{27}$$

where $\theta_{0,U} = u^2/c(0,u)$ and u is the normalized upper clipping bound which is set to 1, for the sake of simplicity. The other required values are defined below.

$$c(0,u) = -\Phi(0) - (u^2-1)\Phi(u) + u^2 - ug(u), \tag{28}$$

$$g(x) = \frac{1}{\sqrt{(2\pi)}}\exp\frac{-x^2}{2}, \quad \Phi(x) = \int_{-\infty}^{x}\frac{1}{\sqrt{2\pi}}\exp\frac{-t^2}{2}dt \tag{29}$$

In order to make DFT precoded OFDM compatible with VLC, we have implemented real and imaginary separation and concept of flip OFDM in order to obtain unipolar signals. It is important to note that the distribution of PAPR will depend upon the instantaneous power and average power. As real and imaginary separation followed by positive and negative separation is implemented, therefore, the relationship between average signal power of x'_n and z_n can be obtained as:

$$E[|x'_n|^2] = 4E[|z_n|^2] \tag{30}$$

The CCDF of PAPR for DP-OOFDM can be obtained by

$$\begin{aligned}\Gamma_{DP-OOFDM} &= \text{Prob}(PAPR_z > \zeta)\\ &= 1-(\text{Prob}(PAPR_z < \zeta))\\ &= 1-\text{Prob}\left(\frac{\max\limits_{0\le n\le 4M-1}|z_n|^2}{E[|z_n|^2]} < \zeta\right)\end{aligned} \tag{31}$$

It is important to note that z_n and z_{n+2M} are correlated i.e. only one of them would be non-zero, however, the same is not true for z_n and z_{n+M}, as they represent the real and imaginary part of x'_n. Therefore, equation (31) can be rewritten as:

$$\begin{aligned}\Gamma_{DP-OOFDM} &= 1-2\times\text{Prob}\left(\max_{0\le n\le 2M-1}|z_n|^2 < \zeta E[|z_n|^2]\right)\\ &= 1-2\times\prod_{n=0}^{2M-1}\text{Prob}\left(x_n'^2 < \frac{\zeta E[(x'_n)^2]}{4}\right)\\ &= 1-2\times\text{Prob}\left(x_n'^2 < \frac{\zeta E[(x'_n)^2]}{4}\right)^{2M}\end{aligned} \tag{32}$$

It may be noted that for localized and interleaved sub-carrier mapping the distribution of instantaneous power of x'_n remains the same [46]. The CDF of instantaneous power of x'_n at a given time instant n can be expressed as [44]:

$$\text{Prob}(x_n'^2 < \xi) = \sqrt{\xi}\int_0^{\infty} J_1(\sqrt{\xi}R)\, G(R,n)\, dR \tag{33}$$

where $J_n(\cdot)$ donates n^{th} order first kind Bessel function and

$$G(R;n) \triangleq \frac{1}{2\pi}\int_0^{2\pi}\mho_{x,y}(R\cos(\phi), R\sin(\phi); n)d\phi \tag{34}$$

here, $\mho_{x,y}$ is the joint characteristic function of $Re(x'_n)$ and $Imag(x'_n)$. For Q^2-QAM, $G(R;n)$ is defined as follows [45]:

$$G(R;n) = \left(\frac{2}{Q}\right)^2\sum_{m=0}^{\frac{Q}{2}-1}\sum_{l=0}^{\frac{Q}{2}-1}J_0\left(\alpha_n R\sqrt{A_m^2+A_l^2}\right) \tag{35}$$

where α_n depends on the pulse shaping filter i.e., $\alpha_n = g(t+nT)$ and $A_m \triangleq (2m+1)\sqrt{\frac{3}{2(Q^2-1)}} : m = \frac{-Q}{2},\ldots,-1,0,\ldots,\frac{Q}{2}$ and $A_l \triangleq (2l+1)\sqrt{\frac{3}{2(Q^2-1)}} : l = \frac{-Q}{2},\ldots,-1,0,\ldots,\frac{Q}{2}$. The PAPR can be calculated by substituting values from equation (33) and (35) into (32).

B. COMPLEXITY

In this section, the system complexities of various modulation schemes are analyzed. The complexity is quantified in terms of the total number of arithmetic operations required at the transceiver. For DFT and IDFT operations, an efficient implementation based on fast Fourier transform (FFT) and inverse FFT (IFFT) algorithms is considered. For N-order FFT/IFFT approximately $4\,N\log_2(N)$ arithmetic operations are required [47]. In case of ACO-OFDM, there is only M-point IDFT, whereas in case of DP-OOFDM there is N-point DFT, M-point IDFT and frequency domain pulse shaping, therefore, the complexity of DP-OOFDM is higher than ACO-OFDM. The G-DP-OOFDM is an attempt to reduce the complexity of DP-OOFDM by using two $N/2$-point DFTs for precoders instead of one N-point DFT precoder, as used in DP-OOFDM. The computational complexities of transmitters for these schemes are given in Table 2. It can be seen that G-DP-OOFDM reduces the computational complexity of system as compared to conventional DP-OOFDM.

TABLE 2. Computational complexity of transmitters for different schemes.

Modulation scheme	No. of effective real multiplications
ACO-OFDM	$4M\log_2(M)$
DP-OOFDM	$4M\log_2(M)+4N\log_2(N)+M^2$
G-DP-OOFDM	$4M\log_2(M)+4N\log_2(N/2)+M^2$

C. SPECTRAL EFFICIENCY

The spectral efficiency of OFDM and DFT precoded OFDM is a function of IDFT size (M) and modulation order (Q). If pulse shaping filter is not considered, then OFDM and DFT precoded OFDM will have same spectral efficiency given as [48]:

$$\eta = Q\frac{M/4}{M+CP} \tag{36}$$

where, the factor of $1/4$ takes into account the loss of spectral efficiency for conversion of complex bipolar signal into real unipolar signal.

However, in the DP-OOFDM system, we have considered a GMSK pulse shaping filter along with DFT precoded OFDM whereas conventional OFDM uses a rectangular pulse, i.e., sinc in frequency domain. The magnitude response of rectangular and GMSK filters are shown in Figs. 5(a) and 5(b) respectively. It is observed that the rectangular filter has higher sidelobes as compared to GMSK filter, therefore, making the proposed DP-OOFDM more spectrally efficient as compared to ACO-OFDM.

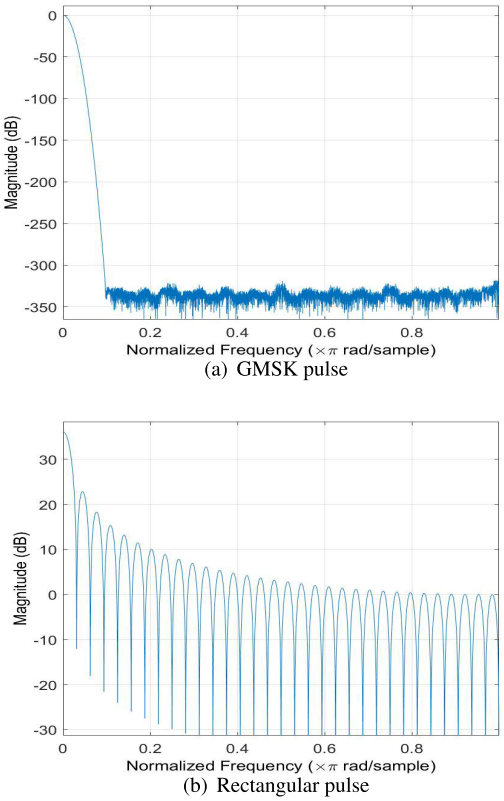

(a) GMSK pulse

(b) Rectangular pulse

FIGURE 5. Magnitude response.

TABLE 3. Simulation parameters.

Parameters	ACO-OFDM	DFT-precoded OFDM	DP-OOFDM	G-DP-OOFDM
Modulation Order	4 QAM	4 QAM	4 QAM	4 QAM
Order of IDFT	64	64	64	64
Pulse shaping filter	Rect.	Rect.	GMSK	GMSK
Bandwidth time product (BT)	NA	NA	0.5	0.5
Precoding	NA	32-point DFT	32-point DFT	$2\times$ 16-point DFT

IV. SIMULATION RESULTS AND DISCUSSION

In this section, different variants of DP-OOFDM are compared with DFT precoded O-OFDM and ACO-OFDM, based on their PAPR, SER and power saving. The channel and simulation parameters are given in Table 1 and Table 3 respectively. The numerical simulation is done using MATLAB software and the variants of DP-OOFDM considered in this work are as follows:

1) **L-DP-OOFDM:** DP-OOFDM with localized subcarrier mapping.
2) **I-DP-OOFDM:** DP-OOFDM with interleaved subcarrier mapping.
3) **G-L-DP-OOFDM:** Grouped DFT precoded DP-OOFDM with localized subcarrier mapping.
4) **G-I-DP-OOFDM:** Grouped DFT precoded DP-OOFDM with interleaved subcarrier mapping.

A. PAPR

The CCDF of PAPR is commonly used to measure the performance of PAPR reduction techniques, which defines the probability of PAPR exceeding a certain threshold value (ζ). Figs. 6(a) and 6(b) show the CCDF of PAPR for DP-OOFDM with localized and interleaved sub-carrier mapping respectively.

For localized mapping Figs. 6(a), it is observed that the proposed L-DP-OFDM, performs better than the L-DFT precoded OOFDM and ACO-OFDM. For a clipping probability Prob($PAPR > \zeta$) $= 10^{-1}$, $PAPR$ gain of 2.5 and 5 dB is achieved in L-DP-OOFDM over L-DFT precoded OOFDM, and ACO-OFDM respectively. Similarly, for interleaved sub-carrier mapping, proposed I-DP-OFDM have superior PAPR performance as compared to I-DFT precoded OOFDM and ACO-OFDM, as shown in Fig. 6(b). $PAPR$ gain of 1.9 and 10.6 dB is achieved by I-DP-OOFDM over I-DFT-precoded OOFDM and ACO-OFDM, if the clipping probability Prob($PAPR > \zeta$) is set to 10^{-1}. It may be noted that the proposed DP-OOFDM provides significantly lower PAPR than ACO-OFDM because of the DFT precoding which results into a system similar to single carrier system, therefore reduces the PAPR.

Moreover, the proposed DP-OOFDM further reduces the PAPR compared to the corresponding DFT-precoded-OOFDM scheme because of the GMSK pulse shaping filter which makes the signal envelope almost constant.

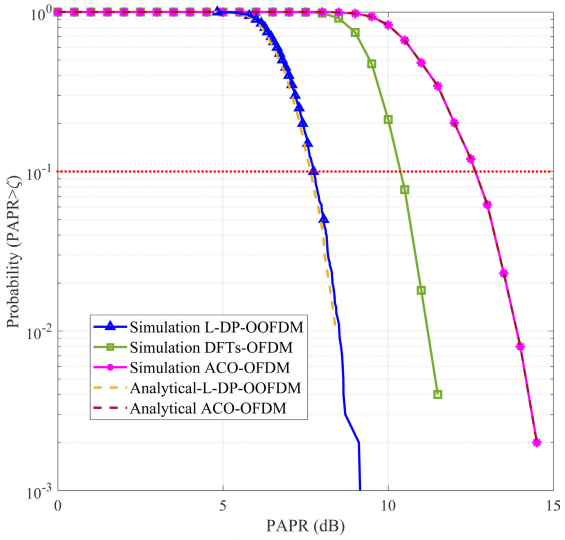

(a) Localized subcarrier mapping

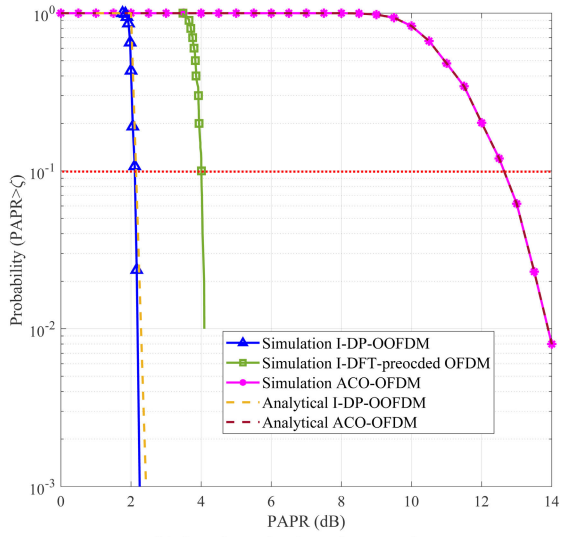

(b) Interleaved subcarrier mapping

FIGURE 6. CCDF distribution of PAPR.

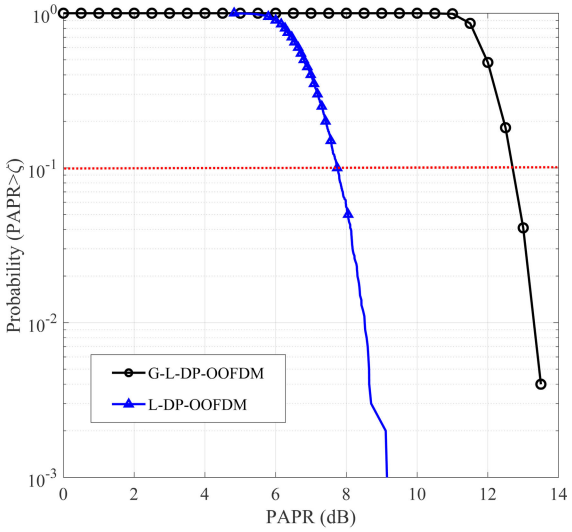

(a) Localized subcarrier mapping

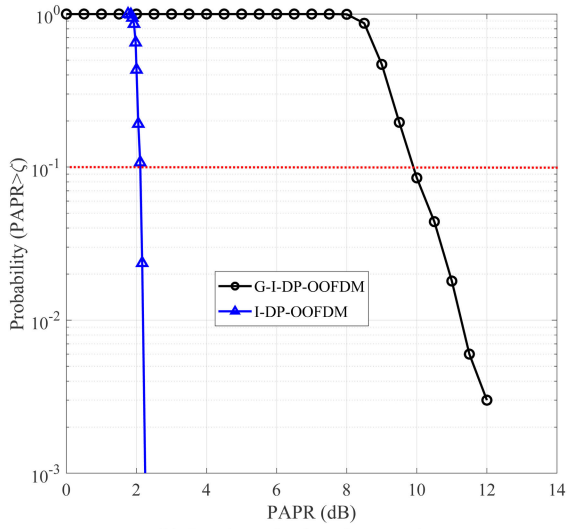

(b) Interleaved subcarrier mapping

FIGURE 7. Effect of grouped DFT precoding on CCDF distribution of PAPR.

The theoretical PAPR derived in section III-A have been plotted in Fig.6, and they show a close overlap with the simulation results.

Fig. 7 illustrates the effect of grouped DFT precoding for the proposed DP-OOFDM in terms PAPR CCDF. It can be clearly seen that the PAPR for grouped configurations are higher as compared to the ungrouped configurations. In case of localized subcarrier mapping, for clipping probability Prob($PAPR > \zeta$) $= 10^{-1}$, the value of $PAPR$ is 5 and 12.5 dB in L-DP-OOFDM and G-L-DP-OOFDM respectively. Similarly, for interleaved subcarrier mapping, at clipping probability Prob($PAPR > \zeta$) $= 10^{-1}$, the value of $PAPR$ is 2.1 and 9.8 dB in I-DP-OOFDM and G-I-DP-OOFDM respectively. This is due to the fact that in G-DP-OOFDM, two 16-point DFTs are applied and the output is multiplexed, followed by pulse shaping and IDFT operation. In this case, the two 16-point DFTs restricts the DFT spread to a lesser number of subcarriers, therefore the overall G-DP-OOFDM signal does not follow single carrier like characteristics, thus resulting into a higher PAPR than the corresponding DP-OOFDM counterpart.

Overall, I-DP-OOFDM provides lowest PAPR as compared to all the other schemes. The reason behind low PAPR of I-DP-OOFDM can be explained by referring to the time domain output structure shown in Fig.3. Because of this structure, interleaved mode output will have less fluctuation and lower peaks than localized mode output. Therefore, the interleaved mode is desirable than the localized mode in terms of PAPR.

B. SER

The SER performance for localized subcarrier mapping (L-DP-OOFDM and L-DFT-precoded OFDM) is shown in Fig. 8(a). It is observed that L-DP-OOFDM have better SER performance compared to ACO-OFDM, and L-DFT precoded OFDM performs better than L-DP-OOFDM, in terms

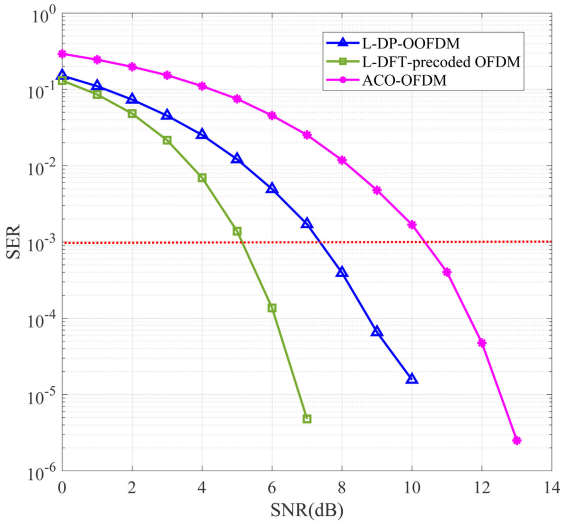

(a) Localized subcarrier mapping

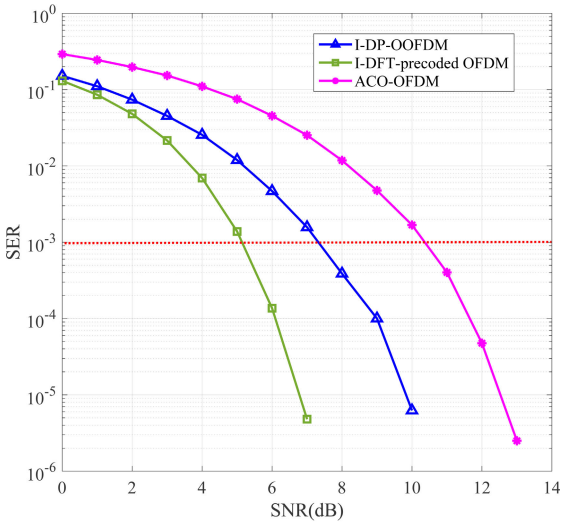

(b) Interleaved subcarrier mapping

FIGURE 8. SER Performance.

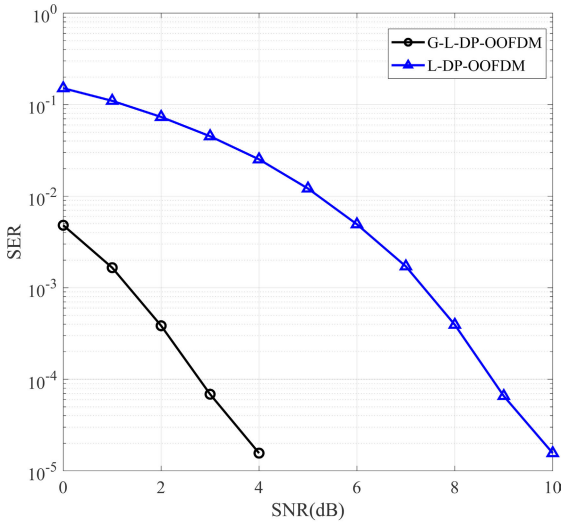

(a) Localized subcarrier mapping

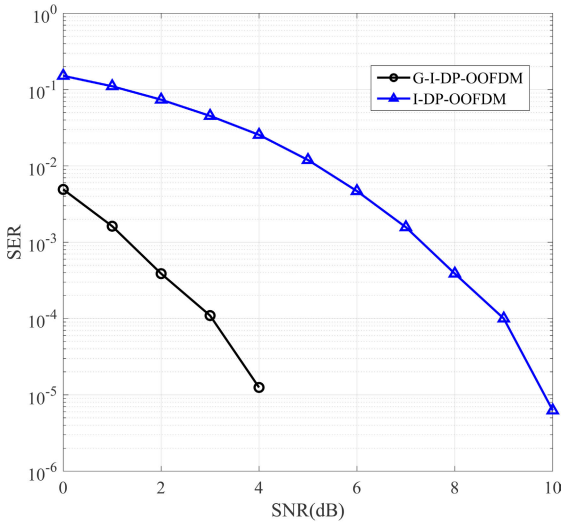

(b) Interleaved subcarrier mapping

FIGURE 9. Effect of grouped DFT precoding on SER Performance.

of SER. For FEC limit i.e., *SER* of 10^{-3}, L-DP-OOFDM provides SNR gain of 2.9 dB over ACO-OFDM, whereas L-DFT-precoded OFDM provides SNR gain of 2.3 dB over L-DP-OOFDM.

Similar trend is observed for Interleaved subcarrier mapping (I-DP-OOFDM and I-DFT-precoded OOFDM) as shown in Fig. 8(b). It is observed that for FEC limit, I-DP-OOFDM and I-DFT-precoded OOFDM provides SNR gain of 2.9 and 5.2 dB over ACO-OFDM respectively. The effect of grouped DFT precoding on SER performance is shown in Fig. 9. In case of localized subcarrier mapping, for FEC limit, G-L-DP-OOFDM provides a SNR gain of 6.1 dB over ACO-OFDM. Similar performance gain is observed for interleaved subcarrier mapping. From the observations, it can be concluded that grouping not only reduces the computational complexity but also improves the SER performance. Further, it is worth noting that the SER performance is independent of the subcarrier mapping.

C. POWER SAVING

The power saving (P_{saving}) achieved by the DP-OOFDM over the ACO-OFDM, is given by

$$P_{saving_{DP-OOFDM}} = 10\log_{10}\left(\frac{P_{ACO-OFDM}}{P_{DP-OOFDM}}\right) \tag{37}$$

where, $P_{ACO-OFDM}$ and $P_{DP-OOFDM}$ corresponds to the power required for the transmission of ACO-OFDM signal and different variants of DP-OOFDM respectively. The values of $P_{ACO-OFDM}$ and $P_{DP-OOFDM}$ can be calculated by using the following generic formula [49].

$$P = P_{avg} * \xi \tag{38}$$

where, ξ is the inverse function of the CCDF for a given clipping probability i.e., Prob.($PAPR > \zeta$) and P_{avg} is the average power per time slot. From simulation results, P_{avg} has been calculated for ACO-OFDM, L-DP-OOFDM, G-L-DP-OOFDM, I-DP-OOFDM and G-I-DP-OOFDM

TABLE 4. Summary of results.

Parameters	ACO-OFDM	Localized subcarrier mapping			Interleaved subcarrier mapping		
		L-DFT-precoded OOFDM	L-DP-OOFDM	G-L-DP-OOFDM	I-DFT-precoded OOFDM	I-DP-OOFDM	G-I-DP-OOFDM
Value of PAPR (ζ) for CCDF prob. $= 10^{-1}$	12.7	10.2	7.7	12.75	4.0	2.1	9.8
Power saving (dB) with respect to ACO-OFDM	–	3.98	8.19	18.05	8.04	13.84	19.19
SNR (dB) for FEC limit (10^{-3})	10.3	5.1	7.4	1.4	5.1	7.4	1.4

schemes. The value of ζ is calculated for clipping probability Prob.($PAPR > \zeta$) set to 10^{-1} from the CCDF curve (Fig. 6 and 7). The power saving is found to be 8.19, 18.05, 13.83 and 19.19 dB over ACO-OFDM for L-DP-OFDM, G-L-DP-OFDM, I-DP-OFDM and G-I-DP-OFDM respectively.

This power saving over ACO-OFDM is because of the low P_{avg} and reduced PAPR of the proposed schemes. It is important to note that grouped DFT precoding further reduces the *Pavg*, therefore, providing higher power saving.

Similarly, the power saving (P_{saving}) achieved by the DFT-precoded OOFDM over the ACO-OFDM, is given by

$$P_{saving_{DFTprecoded}} = 10\log_{10}\left(\frac{P_{ACO-OFDM}}{P_{DFT-precoded}}\right) \quad (39)$$

where, $P_{ACO-OFDM}$ and $P_{DFT-precoded}$ corresponds to the power required for the transmission of ACO-OFDM signal and different variants of DFT-precoded OOFDM respectively. The values of $P_{ACO-OFDM}$ and $P_{DFT-precoded}$ can be calculated by using (38). By following the same procedure, the power saving for L-DFT-precoded OOFDM and I-DFT-precoded OOFDM over ACO-OFDM is found to be 3.98 and 8.04 dB respectively.

V. CONCLUSION

In this paper, we have proposed and evaluated the DP-OOFDM scheme based on complexity, spectral efficiency, PAPR, power-saving, and SER against conventional DFT-precoded OOFDM and ACO-OFDM. A comprehensive summary of the results is presented in Table 4. The proposed DP-OOFDM schemes have low PAPR and high spectral efficiency as compared to DFT-precoded OFDM and ACO-OFDM. The concept of grouped DFT precoding was introduced to reduce the computational complexity of the proposed DP-OOFDM but it resulted in a poorer PAPR performance when compared to the DP-OOFDM. The grouped precoded schemes still provided better power-saving as compared to all the other schemes considered in this paper. It can be concluded that I-DP-OOFDM outperforms all the schemes considered from PAPR perspective, however, G-I-DP-OOFM is preferred from SER and power-saving points of view. Therefore, we can choose G-I-DP-OOFDM for high reliability and power saving, whereas I-DP-OOFDM is the most appropriate scheme for low PAPR applications. These results are useful in selecting relevant schemes for different VLC applications.

ACKNOWLEDGMENT

The authors would like to thank Intel India for PhD fellowship.

REFERENCES

[1] "Cisco visual networking index: Forecast and methodology 2016–2021," V Cisco, San Jose, CA, USA, White Paper, 2017. [Online]. Available: https://www.reinvention.be/webhdfs/v1/docs/complete-white-paper-c11-481360.pdf
[2] L. U. Khan, "Visible light communication: Applications, architecture, standardization and research challenges," *Digit. Commun. Netw.*, vol. 3, no. 2, pp. 78–88, May 2017.
[3] M. Z. Chowdhury, M. K. Hasan, M. Shahjalal, M. T. Hossan, and Y. M. Jang, "Optical wireless hybrid networks: Trends, opportunities, challenges, and research directions," *IEEE Commun. Surveys Tuts.*, vol. 22, no. 2, pp. 930–966, 2nd Quart., 2020.
[4] M. Z. Chowdhury, M. T. Hossan, A. Islam, and Y. M. Jang, "A comparative survey of optical wireless technologies: Architectures and applications," *IEEE Access*, vol. 6, pp. 9819–9840, 2018.
[5] J. Armstrong, "OFDM for optical communications," *J. Lightw. Technol.*, vol. 27, no. 3, pp. 189–204, Feb. 1, 2009.
[6] J. Armstrong and B. Schmidt, "Comparison of asymmetrically clipped optical OFDM and DC-biased optical OFDM in AWGN," *IEEE Commun. Lett.*, vol. 12, no. 5, pp. 343–345, May 2008.
[7] N. Fernando, Y. Hong, and E. Viterbo, "Flip-OFDM for unipolar communication systems," *IEEE Trans. Commun.*, vol. 60, no. 12, pp. 3726–3733, Dec. 2012.
[8] Z. Yu, R. J. Baxley, and G. T. Zhou, "Peak-to-average power ratio and illumination-to-communication efficiency considerations in visible light OFDM systems," in *Proc. IEEE Int. Conf. Acoust., Speech Signal Process.*, May 2013, pp. 5397–5401.
[9] Z.-P. Wang, S.-F. Chen, Y. Zhou, M. Chen, J. Tang, and L. Chen, "Combining discrete cosine transform with clipping for PAPR reduction in intensity-modulated OFDM systems," *Optoelectron. Lett.*, vol. 10, no. 5, pp. 356–359, Sep. 2014.
[10] W. Xu, M. Wu, H. Zhang, X. You, and C. Zhao, "ACO-OFDM-specified recoverable upper clipping with efficient detection for optical wireless communications," *IEEE Photon. J.*, vol. 6, no. 5, pp. 1–17, Oct. 2014.
[11] H. Zhang, L.-L. Yang, and L. Hanzo, "Piecewise companding transform assisted optical-OFDM systems for indoor visible light communications," *IEEE Access*, vol. 5, pp. 295–311, 2017.
[12] D. Abed and A. Medjouri, "Discrete sliding norm transform-based 50% PAPR reduction in asymmetrically clipped optical OFDM systems for optical wireless communications," *Electron. Lett.*, vol. 51, no. 25, pp. 2128–2130, Dec. 2015.
[13] L. Nadal, M. Svaluto Moreolo, J. M. Fabrega, and G. Junyent, "Comparison of peak power reduction techniques in optical OFDM systems based on FFT and FHT," in *Proc. 13th Int. Conf. Transparent Opt. Netw.*, Jun. 2011, pp. 1–4.
[14] J. Bai, Y. Li, Y. Yi, W. Cheng, and H. Du, "PAPR reduction based on tone reservation scheme for DCO-OFDM indoor visible light communications," *Opt. Express*, vol. 25, no. 20, pp. 24630–24638, 2017.
[15] W. O. Popoola, Z. Ghassemlooy, and B. G. Stewart, "Pilot-assisted PAPR reduction technique for optical OFDM communication systems," *J. Lightw. Technol.*, vol. 32, no. 7, pp. 1374–1382, Apr. 1, 2014.
[16] S. B. Slimane, "Reducing the Peak-to-Average power ratio of OFDM signals through precoding," *IEEE Trans. Veh. Technol.*, vol. 56, no. 2, pp. 686–695, Mar. 2007.

[17] R. You and J. M. Kahn, "Average power reduction techniques for multiple-subcarrier intensity-modulated optical signals," in *Proc. IEEE Int. Conf. Commun. ICC. Global Converg. Through Commun. Conf. Rec.*, Jun. 2000, pp. 1620–1627.
[18] J. Zhou and Y. Qiao, "Low-PAPR asymmetrically clipped optical OFDM for intensity-modulation/direct-detection systems," *IEEE Photon. J.*, vol. 7, no. 3, pp. 1–8, Jun. 2015.
[19] A. A. Sharifi, "PAPR reduction of optical OFDM signals in visible light communications," *ICT Express*, vol. 5, no. 3, pp. 202–205, Sep. 2019.
[20] M. A. Aboul-Dahab, A. Esam, and A. A. Elhaseeb, "PAPR reduction based on DFT precoding for OFDM signals," *Int. J. Future Comput. Commun.*, vol. 2, no. 4, p. 325, 2013.
[21] W. Shieh, Y. Tang, and B. S. Krongold, "DFT-spread OFDM for optical communications," in *9th Int. Conf. Opt. Internet (COIN) Dig.*, Jul. 2010, pp. 1–3.
[22] M. Shi, C. Wang, H. Guo, Y. Wang, X. Li, and N. Chi, "A high-speed visible light communication system based on DFT-S OFDM," in *Proc. IEEE Int. Conf. Commun. Syst. (ICCS)*, Dec. 2016, pp. 1–5.
[23] Z.-Y. Wu, Y.-L. Gao, Z.-K. Wang, C. You, C. Yang, C. Luo, and J. Wang, "Optimized DFT-spread OFDM based visible light communications with multiple lighting sources," *Opt. Express*, vol. 25, no. 22, pp. 26468–26482, 2017.
[24] S. B. Slimane, "Peak-to-average power ratio reduction of OFDM signals using pulse shaping," in *Proc. IEEE Global Telecommun. Conf. Conf. Rec. (Globecom)*, 2000, pp. 1412–1416.
[25] G. Huang, A. Nix, and S. Armour, "Impact of radio resource allocation and pulse shaping on papr of SC-FDMA signals," in *Proc. IEEE 18th Int. Symp. Pers., Indoor Mobile Radio Commun.*, Sep. 2007, pp. 1–5.
[26] M. Pervej, T. Roy, and M. Sarker, "PAPR reduction analysis of DFT-SCFDMA system using different pulse shaping filters," in *Proc. Int. Forum Strategic Technol. (IFOST)*, 2014.
[27] M. V. R. Vittal, K. Ramanaidu, and C. Subhas, "PAPR analysis of single carrier FDMA signals with Gaussian pulse shaping," in *Proc. Int. Conf. Commun. Signal Process.*, Apr. 2013, pp. 776–780.
[28] O. Mauritz and B. Popovic, "Optimum family of spectrum-shaping functions for PAPR reduction of DFT-spread OFDM signals," in *Proc. IEEE Veh. Technol. Conf.*, Sep. 2006, pp. 1–5.
[29] H. Myung, J. Lim, and D. Goodman, "Single carrier FDMA for uplink wireless transmission," *IEEE Veh. Technol. Mag.*, vol. 1, no. 3, pp. 30–38, Sep. 2006.
[30] O. Narmanlioglu, R. C. Kizilirmak, and M. Uysal, "The impact of pulse shaping filters on OFDM-based visible light communications," in *Proc. IEEE 10th Int. Conf. Appl. Inf. Commun. Technol. (AICT)*, Oct. 2016, pp. 1–4.
[31] S. B. Slimane, "Peak-to-average power ratio reduction of OFDM signals using broadband pulse shaping," in *Proc. IEEE 56th Veh. Technol. Conf.*, Sep. 2002, pp. 889–893.
[32] K. Kuchi, "Partial response DFT-precoded-OFDM modulation," *Trans. Emerg. Telecommun. Technol.*, vol. 23, no. 7, pp. 632–645, Nov. 2012.
[33] C. Wu, H. Zhang, and W. Xu, "On visible light communication using LED array with DFT-spread OFDM," in *Proc. IEEE Int. Conf. Commun. (ICC)*, Jun. 2014, pp. 3325–3330.
[34] A. W. Azim, Y. Le Guennec, and G. Maury, "Hermitian symmetry free optical-single-carrier frequency division multiple access for visible light communication," *Opt. Commun.*, vol. 415, pp. 177–185, May 2018.
[35] R. Bai, Z. Wang, R. Jiang, and J. Cheng, "Interleaved DFT-spread layered/enhanced ACO-OFDM for intensity-modulated direct-detection systems," *J. Lightw. Technol.*, vol. 36, no. 20, pp. 4713–4722, Oct. 15, 2018.
[36] Z.-P. Wang and S.-Z. Zhang, "Grouped DCT precoding for PAPR reduction in optical direct detection OFDM systems," *Optoelectron. Lett.*, vol. 9, no. 3, pp. 213–216, May 2013.
[37] T. Turletti, "GMSK in a nutshell," Telemedia Netw. Syst. Group LCS, MIT-TR, Tech. Rep., 1996. [Online]. Available: https://d1wqtxts1xzle7.cloudfront.net/36490698/QMSK_in_a_nutshell.pdf?1422895477=&response-content-disposition=inline%3B+filename%3DGMSK_in_a_nutshell.pdf&Expires=1593879768&Signature=dYABOiNw5qHCj1HIwQSlF3EdzYTor-UkVIH6AsNxwTaYJhqHHnYoMBPR0dVRIsriOmAbhPYecK1QsYHVqvMcvOuOy2QTWH~UawD08pwxly9irdnVpxMZnwKfqdknVRL4R7Gq6adgDSkUeAEGswNGqij2rxs1w8nnI5eQcgl2fDRQVTaVKz~x1vjYQ1usipM5rsvjCJCL6DBw3jHn4zKmSTCRtvPA4Xckq0T1xmzIS87SeJAp21wSINQ~jKVSn1PS~ma4hs8SKYAc7ly7E7-Rk-0wH488X8yV-J6OziM5ug5LrQ4D1jfBDjwPQKnCdTx8oaPtaMp948YD3M6mwz2gdQ__&Key-Pair-Id=APKAJLOHF5GGSLRBV4ZA
[38] R. Ahmad, A. Srivastava, and H. A. I. Selmy, "Advanced modulation techniques for low PAPR in VLC system," in *Proc. 20th Int. Conf. Transparent Opt. Netw. (ICTON)*, Jul. 2018, pp. 1–5.
[39] U. Sorger, I. De Broeck, and M. Schnell, "Interleaved FDMA–A new spread-spectrum multiple-access scheme," in *Proc. ICC IEEE Int. Conf. Commun. Conf. Rec. Affiliated (SUPERCOMM)*, Jun. 1998, pp. 1013–1017.
[40] H. Myung, J. Lim, and D. Goodman, "Peak-to-average power ratio of single carrier FDMA signals with pulse shaping," in *Proc. IEEE 17th Int. Symp. Pers., Indoor Mobile Radio Commun.*, Sep. 2006, pp. 1–5.
[41] J. R. Barry, J. M. Kahn, W. J. Krause, E. A. Lee, and D. G. Messerschmitt, "Simulation of multipath impulse response for indoor wireless optical channels," *IEEE J. Sel. Areas Commun.*, vol. 11, no. 3, pp. 367–379, Apr. 1993.
[42] T. Komine and M. Nakagawa, "Performance evaluation of visible-light wireless communication system using white LED lightings," in *Proc. 9th Int. Symp. Comput. Commun. (ISCC)*, Jun. 2004, pp. 258–263.
[43] J. Wang, Y. Xu, X. Ling, R. Zhang, Z. Ding, and C. Zhao, "PAPR analysis for OFDM visible light communication," *Opt. Express*, vol. 24, no. 24, pp. 27457–27474, 2016.
[44] H. Ochiai, "Peak-to-average power ratio distribution analysis of singlecarrier FDMA signals," in *Proc. Eur. Wireless Conf.*, Apr. 2012, pp. 1–5.
[45] H. Ochiai, "Exact and approximate distributions of instantaneous power for pulse-shaped single-carrier signals," *IEEE Trans. Wireless Commun.*, vol. 10, no. 2, pp. 682–692, Feb. 2011.
[46] H. Ochiai, "On instantaneous power distributions of single-carrier FDMA signals," *IEEE Wireless Commun. Lett.*, vol. 1, no. 2, pp. 73–76, Apr. 2012.
[47] S. G. Johnson and M. Frigo, "A modified split-radix FFT with fewer arithmetic operations," *IEEE Trans. Signal Process.*, vol. 55, no. 1, pp. 111–119, Jan. 2007.
[48] R. Gerzaguet, D. Kténas, N. Cassiau, and J. Doré, "Comparative study of 5G waveform candidates for below 6 GHz air interface," in *Proc. ETIs Workshop Future Radio Technol., Focusing Air Interface*, Sophia Antipolis, France, 2016, pp. 1–16.
[49] T.-A. Truong, M. Arzel, H. Lin, B. Jahan, and M. Jezequel, "DFT precoded OFDM—An alternative candidate for next generation PONs," *J. Lightw. Technol.*, vol. 32, no. 6, pp. 1228–1238, Mar. 15, 2014.

RIZWANA AHMAD (Member, IEEE) received the B.Tech. and M.Tech. degrees from the Department of Electronics and Communication Engineering, Aligarh Muslim University (AMU), Aligarh, in 2014 and 2016, respectively. She is currently pursuing the Ph.D. degree with the Department of Electronics and Communication Engineering, IIIT-Delhi. She is also an Intel Research Fellow with the Department of Electronics and Communication Engineering, IIIT-Delhi. Her research interests include visible light communication, light fidelity (Li-Fi), and co-existence of Wi- Fi and Li-Fi networks.

ANAND SRIVASTAVA (Member, IEEE) received the M.Tech. and Ph.D. degrees from IIT Delhi. He had a long stint (∼20 years) with the Center for Development of Telematics (CDOT), the Telecom Research Center of Government of India, where he was the Director and a member of the CDOT Board. During his stay in CDOT, he provided Technical Leadership and Motivation to extremely qualified team of engineers involved in the development of national level projects in the areas of telecom security systems, network management systems, intelligent networks, operations support systems, access networks (GPON), and optical technology-based products. He was with Alcatel-Lucent-Bell Labs, India, as Solution Architect for access and core networks. Before joining IIIT Delhi, he was the Dean and a Professor of the School of Computing and Electrical Engineering, Indian Institute of Technology Mandi, India, and also an Adjunct Faculty of IIT Delhi. Majority of these projects were completed successfully and commercially deployed in the public network. He was also closely involved with ITU-T, Geneva in Study Group 15, and represented India for various optical networking standards meetings. His research works are in the area of optical core and access networks, vehicle to vehicle communications, fiber-wireless (FiWi) architectures, optical signal processing, and visible light communications.